CHEMISTRY OF MATERIALS

pubs.acs.org/cm

Article

The Impact of Structural Distortions on the Magnetism of Double Perovskites Containing $5d^1$ Transition-Metal Ions

Victor da Cruz Pinha Barbosa, Jie Xiong, Phuong Minh Tran, Michael A. McGuire, Jiaqiang Yan, Matthew T. Warren, Rolando Valdes Aguilar, Wenjuan Zhang, Mohit Randeria, Nandini Trivedi, Daniel Haskel, and Patrick M. Woodward*

Cite This: *Chem. Mater.* 2022, 34, 1098−1109

Read Online

ACCESS | Metrics & More | Article Recommendations | Supporting Information

ABSTRACT: Five double perovskites, each containing a transition-metal ion with a $5d^1$ configuration, have been studied to better understand the surprising diversity of magnetic ground states seen in these isoelectronic compounds. Ba_2ZnReO_6 adopts the cubic double perovskite structure and magnetically orders below 16 K, with a canted ferromagnetic structure and a saturated magnetization of ∼0.24 μ_B/Re. X-ray magnetic circular dichroism indicates a substantial orbital moment of approximately 0.4 μ_B/Re that opposes the spin moment. The structures of Ba_2NaOsO_6 (canted ferromagnet, T_C = 7 K) and Ba_2LiOsO_6 (antiferromagnet, T_N = 8 K) are reinvestigated using time-of-flight neutron powder diffraction and found to crystallize with the cubic double perovskite structure. No evidence for a structural distortion can be found in either compound down to 10 K. Ba_2CdReO_6 is also cubic at room temperature but undergoes a structural transition upon cooling below ∼180 K to a tetragonal structure with $I4/m$ symmetry that involves compression of the Re−O bonds that are parallel to the c-axis. Sr_2LiOsO_6 shows a similar tetragonal distortion at room temperature and maintains that structure down to 10 K. Surprisingly, the Os-centered octahedron in Sr_2LiOsO_6 is distorted in the opposite direction, exhibiting an elongation of the Os−O bonds along the c-axis. Differences in the distortions of the octahedra lead to different magnetic ground states, antiferromagnetic (T_N = 4 K) for Ba_2CdReO_6 and spin glass (T_g = 30 K) for Sr_2LiOsO_6. Theoretical modeling shows that the varied magnetic behaviors of double perovskites containing $5d^1$ ions are closely tied to crystallographic distortions. These distortions remove the degeneracy of the 5d t_{2g} orbitals, leading to changes in orbital occupation that ultimately determine which of the several competing magnetic ground states is favored.

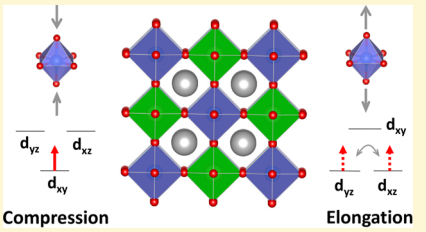

INTRODUCTION

Double perovskites with the general formula $A_2MM'O_6$, where A and M are diamagnetic ions and M′ is a 5d ion, are an intriguing playground for studying magnetism. Two key features—strong spin−orbit coupling and a relatively large radial extension from the nucleus—differentiate 5d orbitals from their 3d counterparts. The former alters the interplay of spin, orbital, charge, and lattice degrees of freedom, while the latter leads to larger hybridization with oxygen, which impacts the strength of competing superexchange interactions and the tendency toward orbital ordering.

Among double perovskites containing M′ cations with either a $5d^2$ or $5d^3$ electron configuration, antiferromagnetic ground states dominate, although recently, three double perovskites containing the $5d^2$ ion Os^{6+} were reported to adopt octupolar ordering rather than conventional long-range ordering of magnetic dipole moments.[1] In contrast, double perovskites containing $5d^1$ ions show a diverse array of ground states (see Figure 1). Previous studies of Ba_2NaOsO_6,[2−4] Ba_2MgReO_6,[5,6] Ba_2ZnReO_6,[5] and Ba_2CdReO_6[7] report a hysteresis loop at a low temperature with a saturated moment of ∼0.2 μ_B per formula unit. Single-crystal magnetization measurements in combination with either nuclear magnetic resonance (NMR)[8] or resonant X-ray scattering studies[9] indicate that the magnetic structures of Ba_2MgReO_6 and Ba_2NaOsO_6 contain ferromagnetic (001) layers that are strongly canted with respect to the neighboring (001) layers. This structure might best be described as intermediate between a colinear ferromagnetic structure and a type I antiferromagnetic structure, as illustrated in Figure 1d. Hereafter, we refer to this as a canted ferromagnetic structure. Ba_2ZnReO_6 and Ba_2CdReO_6 are assumed to adopt similar structures, but magnetization measurements on powder samples are not sufficient to unambiguously differentiate this structure from the simpler ferromagnetic ground state.

Not all $5d^1$ double perovskites adopt the canted ferromagnetic structure of Figure 1d. For reasons that are not well understood, the isoelectronic and isostructural Ba_2LiOsO_6 adopts an antiferromagnetic ground state (T_N =

Received: October 8, 2021
Revised: January 5, 2022
Published: January 19, 2022

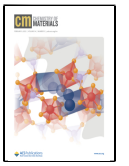

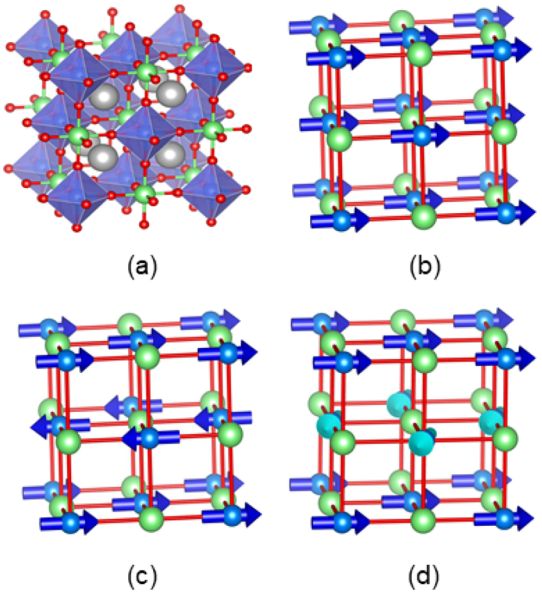

Figure 1. (a) $A_2MM'O_6$ cubic double perovskite structure emphasizing the $M'O_6$ octahedra. Magnetic structures of double perovskites that are (b) ferromagnetic, (c) type I antiferromagnetic, and (d) canted ferromagnetic.

8 K) and has been shown to exhibit a spin-flop transition to a ferromagnetic state in magnetic fields greater than 5.5 T.[2,4] A recent study on single crystals of the tetragonally distorted Sr_2MgReO_6 revealed a type I antiferromagnetic state below T_N = 55 K. Earlier studies on polycrystalline samples of the same compound presented strong evidence for spin glass behavior at a low temperature.[10−13] This suggests that the presence of defects or subtle compositional variations may be enough to stabilize a different magnetic ground state.

A theoretical study of nominally cubic $5d^1$ double perovskites using a model Hamiltonian approach was initiated by Chen et al.[14] and later extended by Svoboda et al.[15] In these studies, two separate phase transitions are found: orbital order (equivalent to quadrupolar order) that sets in at a higher temperature, T_o, and magnetic ordering that occurs at a lower temperature, T_c. This can account for several observed anomalies such as the recovery of only R·ln 2 (and not R·ln 4) entropy at the magnetic T_c in Ba_2NaOsO_6 and Ba_2MgReO_6 and the deviations from the Curie−Weiss susceptibility above T_c. This analysis also shows that the electronically induced orbital ordering naturally leads to a canted ferromagnetic ground state for a large part of parameter space.[14,15] It was also qualitatively argued[15] that the orbital order should lead to a very small lattice distortion, which was difficult to observe directly until the publication of high-resolution, single-crystal diffraction studies of Ba_2MgReO_6.[6,9]

In this study, we take a careful look at the role of structural distortions on the magnetism of double perovskites containing $5d^1$ ions by studying five compositions: Ba_2NaOsO_6, Ba_2LiOsO_6, Ba_2ZnReO_6, Ba_2CdReO_6, and Sr_2LiOsO_6. We find that the latter two compounds undergo tetragonal distortions at temperatures well above the magnetic ordering/freezing temperature, and these distortions have significant implications for the magnetism. Theoretical modeling is used to understand how changes in energy levels and occupation of the 5d orbitals that accompany these structural distortions impact the delicate balance between competing magnetic ground states.

EXPERIMENTAL SECTION

Polycrystalline samples were prepared by solid-state methods. Reagents included BaO (Sigma-Aldrich, 99.99% metals basis), SrO (Sigma-Aldrich, 99.9% trace metals basis), Os powder (Sigma-Aldrich, 99.9% trace metals basis), ReO_3 (Alfa Aesar, 99.9% trace metals basis), ZnO (Alfa Aesar, 99.99% metals basis), CdO (Cerac, 99.95% pure), Li_2O (Alfa Aesar, 99.5%), and Na_2O_2 (Alfa Aesar, 95%). Stoichiometric amounts of the appropriate starting materials were thoroughly mixed using a mortar and pestle in an argon-filled glovebox. The mixture was loaded into an alumina container and sealed in a silica tube under dynamic vacuum. The tube was then placed in a furnace and heated to 1000 °C for 24−48 h. For the compounds containing osmium, a separate alumina cap containing MnO_2 was also enclosed in the sealed quartz tube as the decomposition of MnO_2 acted as the oxygen source needed to oxidize Os metal via reaction 3 $MnO_2(s) \rightarrow Mn_3O_4(s) + O_2(g)$. The amount of MnO_2 used was sufficient to produce 1/4 mole excess $O_2(g)$ for every mole of double perovskite formed. The furnace was located inside a fume hood so that toxic $OsO_4(g)$ would be vented out of the laboratory should the integrity of the silica tube be compromised during heating.

Laboratory X-ray powder diffraction (XRPD) was performed at room temperature using a Bruker D8 Advance diffractometer equipped with a Cu source and a Ge (111) incident beam monochromator. The low-temperature X-ray powder diffraction measurements were performed using a PANalytical X'Pert Pro MPD diffractometer with copper $K\alpha_1$ radiation and an Oxford Phenix cryostat between 20 and 300 K. Synchrotron X-ray powder diffraction data were collected on Ba_2ZnReO_6 and Ba_2CdReO_6 at temperatures of 300 and 90 K using the 11-BM beamline at the Advanced Photon Source, with a wavelength λ = 0.4147 Å. Synchrotron X-ray powder diffraction data were collected on Sr_2LiOsO_6 at 300 K using the Brockhouse X-ray diffraction and scattering beamline (BXDS-WLE) at the Canadian Light Source, with wavelength λ = 0.82015 Å.

Time-of-flight neutron powder diffraction (TOF-NPD) data were obtained on all three osmium-containing double perovskites using the POWGEN diffractometer at the Spallation Neutron Source (SNS) located at Oak Ridge National Laboratory. Approximately 3 g of Ba_2NaOsO_6, 3 g of Ba_2LiOsO_6, and 6 g of Sr_2LiOsO_6 were packed in the cylindrical vanadium cans 6 to 8 mm in diameter. Data were collected with scan times ranging from 30 to 120 min per scan. Constant wavelength neutron powder diffraction (NPD) data sets were collected on Ba_2ZnReO_6 using the triple-axis spectrometer HB-1A at the High Flux Isotope Reactor (HFIR) to look for signs of magnetic scattering. Approximately 11 g of powdered sample was sealed into a cylindrical aluminum can under a He atmosphere. Data were collected at 1.5 and 25 K using constant wavelength neutrons (λ = 2.37 Å) and collimation of 40′-40′-80′-open. The X-ray and neutron diffraction patterns were analyzed using the Rietveld method, as implemented in either the TOPAS-Academic (v6) package[16] or the Fullprof software package.[17]

DC magnetic susceptibility for all samples were measured using a Quantum Design Magnetic Property Measurement System (MPMS) SQUID magnetometer. Polycrystalline samples of approximately 0.1 g were encapsulated in gel capsules, which were inserted into the center of a straw and then mounted in the magnetometer. Data were collected between 2 and 400 K under both zero-field-cooled (ZFC) and field-cooled (FC) conditions with an applied field of 1000 Oe. A diamagnetic correction was applied by subtracting the temperature-dependent susceptibility measured on an empty gel capsule and the diamagnetic constant of the constituent ions.[18] Isothermal magnetization curves were measured between −7 and +7 T. The temperature-dependent specific heat data were collected using a 9 T Quantum Dynamics PPMS in the temperature range 1.9 K < T < 300 K.

https://doi.org/10.1021/acs.chemmater.1c03456
Chem. Mater. 2022, 34, 1098−1109

Table 1. Summary of Key Structural Parameters for the Double Perovskites Studied at Room Temperature[a]

compound	tolerance factor	space group	lattice parameters (Å)	Os/Re−O dist. (Å)	M−O dist. (Å)
Ba_2ZnReO_6	1.041	$Fm\bar{3}m$	a = 8.10610(1)	1.941(1) × 6	2.112(1) × 6
Ba_2LiOsO_6	1.036	$Fm\bar{3}m$	a = 8.10148(2)	1.8964(9) × 6	2.1543(9) × 6
Ba_2CdReO_6	0.990	$Fm\bar{3}m$	a = 8.32557(1)	1.906(3) × 6	2.257(3) × 6
Ba_2NaOsO_6	0.974	$Fm\bar{3}m$	a = 8.28137(2)	1.8829(7) × 6	2.2575(7) × 6
Sr_2LiOsO_6	0.977	$I4/m$	a = 5.52746(4)	1.877(9) × 4	2.053(9) × 4
			c = 7.97506(6)	1.889(7) × 2	2.098(7) × 2

[a]Values based on analysis of either synchrotron X-ray diffraction data (Ba_2ZnReO_6, Ba_2CdReO_6, and Sr_2LiOsO_6) or time-of-flight neutron powder diffraction data (Ba_2LiOsO_6 and Ba_2NaOsO_6). Full details of these refinements can be found in the Supporting Information.

X-ray magnetic circular dichroism (XMCD) data at Re $L_{2,3}$ edges were collected on a powder sample of Ba_2ZnReO_6 using transmission geometry at beamline 4-ID-D of the Advanced Photon Source at Argonne National Laboratory. The helicity of circularly polarized X-rays, generated by a 500 μm-thick diamond (111) phase plate, was switched at 13.1 Hz and the related modulation in X-ray absorption was detected with a phase lock-in amplifier. The sample was mounted in the variable temperature insert of a cryomagnet and cooled to 2 K in ^{4}He vapor. Measurements were done in 4 T applied field for two opposite field directions. The spectra for opposite field directions were combined to yield artifact-free XMCD data. The spectra collected at the L_3 and L_2 edges were normalized and integrated for sum rules analysis.[19,20]

Time-domain terahertz spectroscopy data sets were collected, as described in earlier works by Mai et al. and Warren et al.[21,22] Electrical conductivity was measured on cold-pressed pellets of Ba_2ZnReO_6 and Ba_2CdReO_6 using a Quantum Design Physical Property Measurement System (PPMS). The four-point probe geometry was made using copper wire and silver paint. The low temperature limit is determined by the temperature below which the sample becomes too resistive to be measured accurately.

RESULTS

Room-Temperature Crystal Structures. The crystal structures of Ba_2MOsO_6 (M = Li and Na), Ba_2MReO_6 (M = Zn and Cd), and Sr_2LiOsO_6 were studied using a combination of synchrotron X-ray powder diffraction and neutron powder diffraction techniques. Table 1 summarizes the results at room temperature, where all four barium-containing compounds adopt the cubic double perovskite structure with $Fm\bar{3}m$ space group symmetry. The values of the cell parameters and bond distances for the first four compounds are all in very good agreement (within 1% or less) with earlier literature reports.[2,5,7,23] To a first approximation, the osmium- and rhenium-centered octahedra are similar in size so that the variations in the cubic cell edge largely depend upon the size of the diamagnetic M cation. Those compounds containing Li^+ and Zn^{2+} ions have smaller unit cells, whereas incorporation of larger Na^+ and Cd^{2+} results in a 2−3% expansion of the unit cell edge. As the unit cell expands, the Os−Os and Re−Re distances also increase, which should lead to slightly weaker superexchange coupling between magnetic 5d ions and weaker Coulombic repulsions between the electrons in occupied 5d orbitals on neighboring Os/Re ions. Attempts to refine antisite disorder between octahedral-site cations did not lead to an improvement in the goodness of fit. If antisite disorder is present, it is too small to be detected by diffraction methods. Given the large differences in the charge and size of the M and M′ cations, the absence of antisite disorder is not surprising.

The fit of the Ba^{2+}/Sr^{2+} ions to the cubic network of corner-sharing octahedra can be assessed with the tolerance factor $\tau = \sqrt{2}(r_A + r_O)/(r_M + r_{M'} + 2r_O)$,[24] where $r_{M'}$ is the ionic radius of the osmium/rhenium ion, r_O is the radius of the oxide anion, and r_A and r_M are the radii of 12- and 6-coordinate diamagnetic cations, respectively. We see that for M = Li^+ and Zn^{2+}, the tolerance factor is larger than 1, indicating that the Ba^{2+} ion is stuffed into a framework for which it is slightly too large. This leads to a subtle expansion of the Re−O and Os−O bonds. The effect is surprisingly large for Ba_2ZnReO_6, although it should be noted that an earlier neutron powder study of this compound by Marjerrison et al. reported a somewhat shorter Re−O bond length of 1.922(2) Å.[5] Nevertheless, either value would represent an expansion from the 1.906(3) Å value obtained for Ba_2CdReO_6. This stretching of the bonds will lead to a small reduction in the crystal field splitting of the 5d orbitals and may subtly reduce the covalency of the Re/Os−O bonds.

Unlike its $Ba_2MM'O_6$ counterparts, Sr_2LiOsO_6 is tetragonally distorted from the cubic structure at room temperature, in contradiction to an earlier study that reported a cubic $Fm\bar{3}m$ structure.[25] The magnitude of the distortion can be quantified by the c/a ratio of the original cubic unit cell, which when expressed in terms of the tetragonal unit cell parameters, becomes $c_t/(\sqrt{2}a_t) = 1.020$. This 2% expansion of the c-axis leads to a peak splitting that is evident in both X-ray and neutron diffraction patterns (Figure 2). The tetragonal space

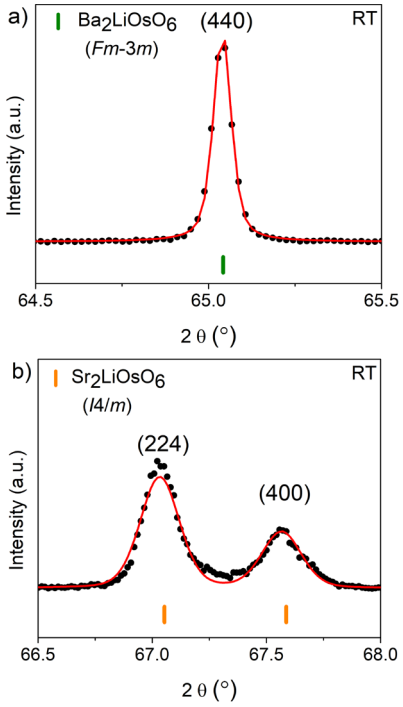

Figure 2. (a) The (440) peak in cubic $Fm\bar{3}m$ Ba_2LiOsO_6 splits into the (b) (224) and (400) peaks in tetragonal $I4/m$ Sr_2LiOsO_6.

https://doi.org/10.1021/acs.chemmater.1c03456
Chem. Mater. 2022, 34, 1098−1109

Table 2. Summary of Key Structural Parameters Obtained from Synchrotron X-ray Powder Diffraction (SXPD), Constant Wavelength Neutron Powder Diffraction (NPD), and Time-of-Flight Neutron Powder Diffraction (TOF-NPD) Data[a]

compound	technique	temp (K)	space group	lattice parameters (Å)	Os/Re−O dist. (Å)	M−O dist. (Å)
Ba_2ZnReO_6	SXPD	90	$Fm\bar{3}m$	a = 8.08998(1)	1.940(1) × 6	2.105(1) × 6
Ba_2ZnReO_6	NPD	25	$Fm\bar{3}m$	a = 8.0940(5)	1.918(3) × 6	2.129(3) × 6
Ba_2ZnReO_6	NPD	1.5	$Fm\bar{3}m$	a = 8.094(1)	1.920(3) × 6	2.127(3) × 6
Ba_2LiOsO_6	TOF-NPD	90	$Fm\bar{3}m$	a = 8.08256(1)	1.8951(8) × 6	2.1462(8) × 6
Ba_2LiOsO_6	TOF-NPD	10	$Fm\bar{3}m$	a = 8.07919(1)	1.8946(8) × 6	2.1450(8) × 6
Ba_2CdReO_6	SXPD	90	$I4/m$	a = 5.87193(7)	1.916(9) × 4	2.25(1) × 4
				c = 8.3236(1)	1.901(7) × 2	2.261(7) × 2
Ba_2NaOsO_6	TOF-NPD	90	$Fm\bar{3}m$	a = 8.26077(2)	1.8829(5) × 6	2.2475(5) × 6
Ba_2NaOsO_6	TOF-NPD	10	$Fm\bar{3}m$	a = 8.25622(1)	1.8834(5) × 6	2.2447(5) × 6
Sr_2LiOsO_6	TOF-NPD	90	$I4/m$	a = 5.4966(1)	1.889(3) × 4	2.032(3) × 4
				c = 8.0034(2)	1.916(4) × 2	2.086(4) × 2
Sr_2LiOsO_6	TOF-NPD	10	$I4/m$	a = 5.49088(1)	1.888(3) × 4	2.031(3) × 4
				c = 8.0111(2)	1.919(4) × 2	2.087(4) × 2

[a]Full details of these refinements can be found in the Supporting Information.

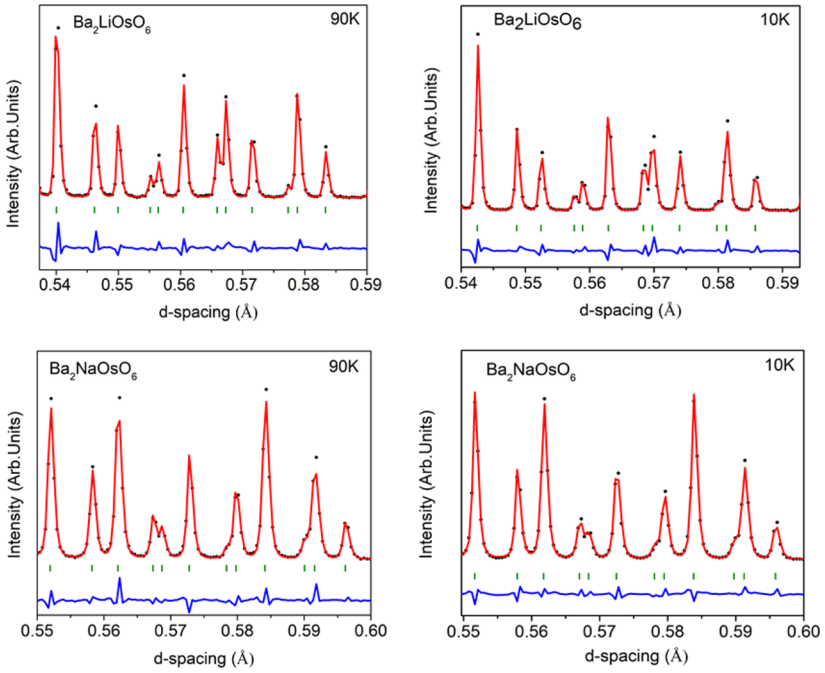

Figure 3. Rietveld refinements of TOF-NPD data collected on Ba_2LiOsO_6 (top) and Ba_2NaOsO_6 (bottom) at 90 K (left) and 10 K (right). The black dots represent experimental intensities, the red line is the fit to the data with a cubic model, the green tick marks denote the expected peak positions, and the blue curve is the difference between experiment and the calculated fit.

group $I4/m$ allows for distortions of the octahedra as well as out-of-phase rotations of the octahedra about the c-axis (Glazer tilt system $a^0a^0c^-$).[26] From the bond lengths in Table 1, we see a 2.2% elongation of the axial bonds of the Li-centered octahedron, whereas the axial bonds of the Os-centered octahedron only elongate by 0.6%. This would seem to suggest that the distortion is driven by the small tolerance factor and the need to optimize the Sr−O bonding, rather than an electronically driven distortion arising from the partially filled t_{2g} orbitals on Os^{7+}. The Os−O−Li bond angle in the ab-plane, which would be linear in the cubic structure, is reduced to 167.9(5)° by rotations of the octahedra. The rotations of Os-centered octahedra as well as the elongation of the c-axis make the superexchange interactions within the ab-plane subtly different than the interactions between different (001) planes, presumably reducing the frustration of the face-centered cubic topology.

Crystal Structures below Room Temperature. Table 2 summarizes the results of low-temperature structural studies carried out using a combination of synchrotron X-ray and neutron powder diffraction methods. No evidence of a reduction in symmetry from the cubic double perovskite structure was detected in Ba_2ZnReO_6, Ba_2LiOsO_6, or Ba_2NaOsO_6. Sr_2LiOsO_6 retains its tetragonal structure down to 10 K, but the tetragonal elongation of the OsO_6 octahedron increases at low temperatures. Ba_2CdReO_6 is the only compound of these five that undergoes a detectable structural phase transition, undergoing a cubic-to-tetragonal phase transition upon cooling below approximately 170−180 K, as discussed below.

Given the relatively large tolerance factors of Ba_2ZnReO_6 (τ = 1.041) and Ba_2LiOsO_6 (τ = 1.036), it is not surprising that the cubic $Fm\bar{3}m$ structure is retained at low temperatures. However, a recent single-crystal synchrotron X-ray diffraction

https://doi.org/10.1021/acs.chemmater.1c03456
Chem. Mater. 2022, 34, 1098−1109

investigation of Ba_2MgReO_6 (τ = 1.046) detected a transition to the tetragonal space group $P4_2/mnm$ below 33 K. This transition appears to be driven by a complex pattern of orbital ordering.[9] SXPD data collected on Ba_2ZnReO_6 at 90 K shows little change from the cubic structure seen at room temperature. NPD data sets collected on the triple-axis spectrometer HB-1A above (25 K) and below (1.5 K) T_C also show no sign of deviation from cubic symmetry, but the relatively low resolution of this instrument is not sufficient to detect the symmetry breaking reported for Ba_2MgReO_6.

High-resolution TOF-NPD data, better suited to detect subtle crystallographic distortions, were collected for the three osmate double perovskites studied. Rietveld refinements using data collected at 10 K are shown in Figure 3. The pattern collected on Ba_2LiOsO_6 was fit with both cubic ($Fm\bar{3}m$) and tetragonal ($P4_2/mnm$) space groups, the latter derived from the low-temperature tetragonal structure of Ba_2MgReO_6.[9] When refined with a tetragonal model, the degree of distortion at 10 K is very small (c/a = 1.0004) but comparable to the values reported for Ba_2MgReO_6 (c/a = 1.0008). However, there is no sign of peak splitting and/or superlattice reflections within the d-space range of the data (0.502−3.106), and the goodness of fit only shows marginal improvement on lowering the symmetry from $Fm\bar{3}m$ (R_{wp} = 4.65%) to $P4_2/mnm$ (R_{wp} = 4.43%). Furthermore, refinements of the 90 K data using a tetragonal model produce a comparable degree of distortion (c/a = 1.0004). Thus, we find no evidence of a tetragonal distortion at 10 K using high-resolution neutron data, but neither can we definitively rule out a very small distortion similar to the one reported in single-crystal studies of Ba_2MgReO_6.

The smaller tolerance factor of Ba_2NaOsO_6 (τ = 0.974) makes a phase transition to tetragonal symmetry more likely. Its tolerance factor is comparable to Sr_2LiOsO_6 (τ = 0.977), and as discussed above, the latter is already tetragonally distorted at room temperature. Furthermore, ^{23}Na NMR studies reported breaking of the cubic symmetry below 13 K in Ba_2NaOsO_6, creating two distinct orthorhombically distorted Na sites.[8,27] Despite the fact that the 10 K data are in the regime that Lu et al. refer to as the broken local point symmetry (BLPS) phase, the time-of-flight NDP data collected at 10 K were well fit by the cubic $Fm\bar{3}m$ space group. As with Ba_2LiOsO_6, it is not possible to categorically rule out a small tetragonal distortion, similar to the one reported for Ba_2MgReO_6, but neither is there any visible evidence of such a distortion in our data.

TOF-NPD data for Sr_2LiOsO_6 collected at 90 and 10 K were refined with the tetragonal $I4/m$ space group seen at room temperature. Fits to the data can be found in the Supporting Information. Upon cooling, the a-axis contracts while the c-axis expands, increasing the tetragonal distortion of the unit cell. The tetragonal distortion of the Os-centered octahedron increases in a similar manner. The Os−O bond distances in the ab-plane—1.889(3) Å at 90 K and 1.888(3) Å at 10 K—are similar to the Os−O bond lengths seen in Ba_2LiOsO_6 and Ba_2NaOsO_6. However, the axial Os−O bonds are clearly elongated, with values of 1.916(4) Å at 90 K and 1.919(4) Å at 10 K. In percentage terms, the axial bonds are elongated with respect to the equatorial bonds by 0.6% at 300 K, 1.4% at 90 K, and 1.6% at 10 K. A similar elongation of the axial bonds has been reported in the isoelectronic and isostructural Sr_2MgReO_6 at a low temperature.[11,28]

The large neutron absorption cross section of Cd prevented neutron studies of Ba_2CdReO_6, but variable temperature laboratory XRPD data collected on a sample of Ba_2CdReO_6 show splitting of the (440) peak into a doublet below 100 K, signifying a cubic-to-tetragonal phase transition (Figure 4).

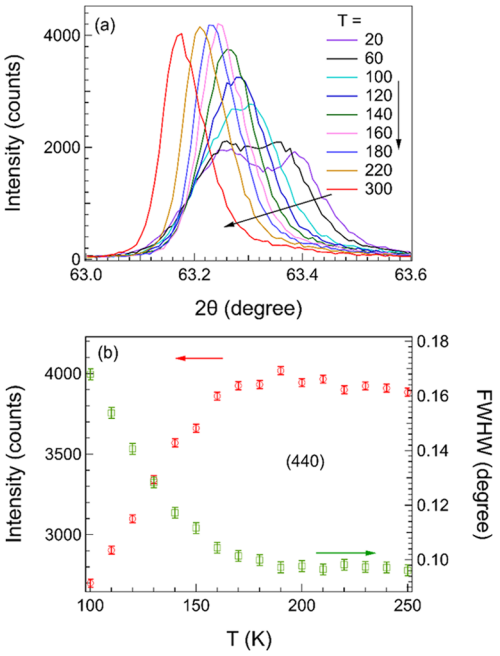

Figure 4. (a) Variable temperature laboratory XRPD data for Ba_2CdReO_6 revealing a splitting of the (440) peak as the temperature is lowered. The arrow shows the direction the peak shifts as the temperature is lowered. (b) Temperature dependence of the maximum intensity and FWHM of the (440) peak.

The FWHM of this peak starts to show signs of broadening at higher temperatures, roughly 170 to 180 K. This is in good agreement with recent studies by Hirai and Hiroi, who also observed a cubic-to-tetragonal phase transition at 170 K.[7] Fits to synchrotron X-ray powder diffraction patterns at 90 K clearly reveal the tetragonal distortion, which can be modeled with the $I4/m$ structure of Sr_2LiOsO_6 (Figure 5). Although the two tetragonal structures share the same space group symmetry, the Re-centered octahedra are distorted in the opposite direction than are the Os-centered octahedra in Sr_2LiOsO_6. The Re−O bonds parallel to the c-axis are shorter, 1.895(6) Å, than those that lie in the ab-plane, 1.926(8) Å. The opposite direction of the tetragonal distortion is also evident in the distortion of the unit cell. The magnitude of the tetragonal distortion for Ba_2CdReO_6 at 90 K, $c_t/(\sqrt{2}a_t)$ = 1.002, is much smaller than the comparable metric in Sr_2LiOsO_6 at 90 K, $c_t/(\sqrt{2}a_t)$ = 1.030. An analogous $Fm\bar{3}m$-to-$I4/m$ structural phase transition resulting in compressed ReO_6 octahedra has been reported in the isoelectronic compound Ba_2CaReO_6 near 120 K.[29]

No sign of magnetic Bragg reflections was observed in any of the samples studied by low-temperature neutron diffraction. While the TOF-NPD data collected on POWGEN are not ideal for observing weak magnetic reflections, the same cannot be said for the constant wavelength data obtained for Ba_2ZnReO_6. The triple-axis spectrometer HB-1A at Oak Ridge National Laboratory is well suited to detect weak magnetic reflections owing to its excellent signal-to-noise ratio,

https://doi.org/10.1021/acs.chemmater.1c03456
Chem. Mater. 2022, 34, 1098−1109

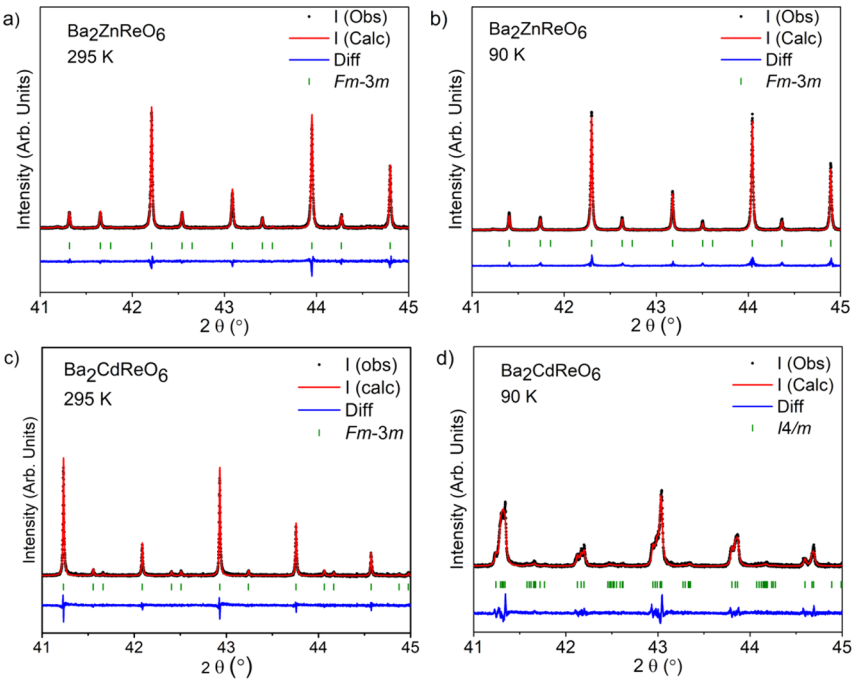

Figure 5. Selected regions of the synchrotron XRD patterns of (a, b) Ba_2ZnReO_6 and (c, d) Ba_2CdReO_6 at 295 and 90 K. The experimental points are represented by black dots, while red and blue lines show the calculated and difference curves. Green tick marks indicate the positions of the allowed peaks.

arising from the combined use of a double-bounce monochromator and an analyzer. Figure 6 shows the

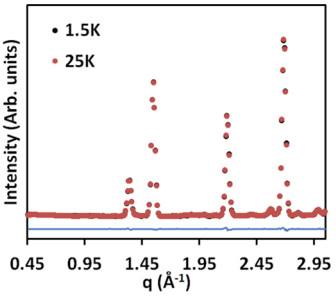

Figure 6. Comparison of the neutron diffraction pattern above (25 K) and below (1.5 K) the Curie transition temperature in Ba_2ZnReO_6. Black and red dots are data collected at 1.5 and 25 K, respectively, and the blue curve is the difference between the two.

comparison between data collected above (25 K) and below (1.5 K) the Curie temperature. Even though no obvious difference is observed, this result should not be taken as evidence against long-range magnetic ordering. The ordered moments of oxides containing $5d^1$ ions are sufficiently small; they can fall below the detection limit. The moment of 0.6 μ_B seen on the same instrument for the $5d^2$ ion Re^{5+} in Ba_2LuReO_6 was not far above the detection limit.[30]

Electrical Conductivity. Previous studies of $A_2MM'O_6$ (M′ = Os, Re) double perovskites, where M is a diamagnetic main group ion, have consistently found activated electrical transport.[3,6,7] Given the open-shell configuration of the Os^{7+} and Re^{6+} ions, Mott insulating behavior is implied. To confirm similar behavior in the compounds discussed here, the electric conductivity of Ba_2ZnReO_6 and Ba_2CdReO_6 was measured as a function of temperature. As shown in Figure 7, the conductivity increases with increasing temperature, confirming

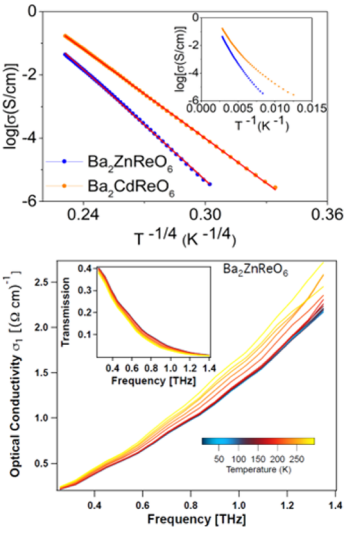

Figure 7. Electric conductivity of Ba_2ZnReO_6 and Ba_2CdReO_6 (top). The inset is the log σ as a function of T^{-1}. Time domain terahertz spectroscopy on Ba_2ZnReO_6 as a function of frequency and temperature (bottom).

the insulating nature of both materials. The conductivity can be fit to a 3D Mott variable range hopping transport model, where log σ is a linear function of $T^{-1/4}$. Attempts to fit the conductivity to a simple Arrhenius model (log σ vs T^{-1}) were not successful.

Electrical transport measurements on polycrystalline pellets can be complicated by resistance at grain boundaries. To confirm the insulating nature of the bulk, time-domain terahertz spectroscopy (TDTS), which is sensitive both to surface and bulk properties, was performed on Ba_2ZnReO_6. TDTS on a polycrystalline pellet of Ba_2ZnReO_6 reveals behavior indicative of a small gap insulator in the approximate

https://doi.org/10.1021/acs.chemmater.1c03456
Chem. Mater. 2022, 34, 1098−1109

frequency range of 0.25−1.5 THz, with conductivity increasing as the temperature increases (Figure 7). The observation of increasing conductivity with increasing frequency is consistent with the variable range hopping behavior observed in the resistivity data. In general, little temperature dependence beyond increasing conductivity with temperature could be discerned.

Specific Heat. The onset of long-range magnetic order in Ba_2ZnReO_6 is confirmed by the anomaly present at 16 K in its specific heat (Figure 8). The transition temperature agrees well

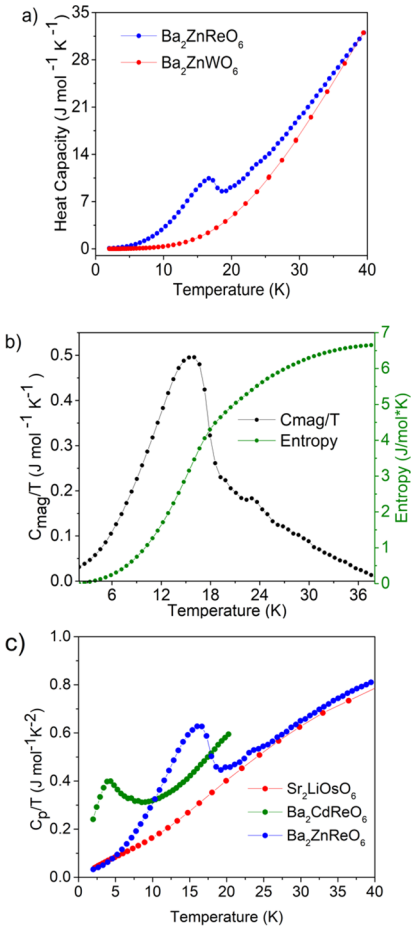

Figure 8. (a) Heat capacity and (b) magnetic contribution to the heat capacity and entropy release for Ba_2ZnReO_6. (c) C_p/T for Ba_2ZnReO_6, Ba_2CdReO_6, and $Sr_2LiOsOsO_6$.

with the magnetometry result discussed below. In addition, there is a very small feature at 23 K that, by analogy with specific heat data collected on Ba_2MgReO_6, may indicate a transition into an orbitally ordered state.[6] To estimate the magnetic contribution, the lattice part of the specific heat was subtracted using data measured on the isostructural double perovskite Ba_2ZnWO_6. An integration of the magnetic specific heat yields an entropy release of 6.7 J/(mol·K). Thus, we recover an S_{mag} that is intermediate between the pure spin limit ($S = 1/2$) of $R\cdot\ln(2S + 1) = R\cdot\ln(2) = 5.76$ J/(mol·K) and the full spin−orbit coupling limit ($J = 3/2$) of $R\cdot\ln(2J + 1) = R\cdot\ln(4) = 11.52$ J/(mol·K). The Ba_2CdReO_6 data show an unmistakable peak at 4 K that signals the onset of long-range magnetic order.

Magnetometry. The sharp rise in zero-field-cooled (ZFC) and field-cooled (FC) susceptibility observed at ∼16 K (Figure 9a), as well as the hysteresis seen at 2 K in the isothermal magnetization data (Figure 9f), indicates a ferromagnetic or canted-ferromagnetic ground state for Ba_2ZnReO_6. The transition temperature T_C = 16 K is determined from the dip in the derivative of the susceptibility and this value agrees well with the feature in the specific heat (Figure 8). The saturated moment at 2 K is ∼0.24 μ_B/formula unit (f.u.), about double the previously reported value.[5]

The temperature-dependent magnetic susceptibility of Ba_2CdReO_6 shows a rise at temperatures below 10 K (Figure 9b). While this rise could signal many things, the presence of a peak in the specific heat (Figure 8c), taken together with the observation that the isothermal magnetization at 2 K is linear (Figure 9f), suggests antiferromagnetic ordering, with T_N = 4 K. Unlike the resistivity and structural characterization discussed above, this result does not agree with the recent study of Hirai and Hiroi. They observed a clear hysteresis at 2 K, consistent with the canted ferromagnetic structure (Figure 1d), and reported an ordering temperature of 12 K.[7]

A sharp rise in magnetization near 7 K is observed for Ba_2NaOsO_6 (Figure 9c). This feature, together with the hysteresis seen in the isothermal magnetization at 2 K (Figure 9f), is consistent with previous reports of canted ferromagnetism.[2,8,27] The saturation magnetization is approximately 0.11 μ_B/f.u., which is smaller by a factor of approximately 2 than the values reported in the literature. A previous report indicates that Ba_2LiOsO_6 has an antiferromagnetic ground state with $T_N \approx 8$ K.[2] The temperature-dependent magnetization data (Figure 9d) do not show a clear cusp indicative of the onset of long range order, but the linear magnetization as a function of applied field at 2 K is at least consistent with antiferromagnetism. Unlike the other compounds studied, there is minimal divergence between FC and ZFC curves, which is also consistent with antiferromagnetic ordering. The temperature dependent magnetization of Sr_2LiOsO_6 shows an antiferromagnetic-like cusp at 30 K. However, the absence of anomaly in the specific heat data (vide infra) suggests that the cusp corresponds to freezing of spins into a glassy state. This would be consistent with the significant divergence seen between the zero-field-cooled and field-cooled curves.

The inverse susceptibility in the high-temperature paramagnetic region can be fit to a linear Curie−Weiss plot provided that a temperature-independent parameter (TIP) is included in the fit:

$$\chi = \frac{C}{(T - \theta)} + \chi_0$$

where χ represents magnetic susceptibility, T represents the temperature, C represents the Curie constant, θ represents the Weiss constant, and χ_0 represents the temperature-independent correction. Given the small sizes of the magnetic moments in these compounds, the Curie−Weiss plots are in general not very linear unless one is careful to subtract out the diamagnetic contribution of the core electrons (which has been done) and include a TIP.[31] From the Curie−Weiss plots, shown in the Supporting Information, the effective moments and Weiss constants can be extracted (see Table 3). The Weiss constant is negative for all five compounds, even Ba_2ZnReO_6 and Ba_2NaOsO_6, which are nearly ferromagnetic, as discussed in the Introduction. Not surprisingly, the effective moments are significantly reduced from the spin-only value of 1.73 μ_B. The observation that the effective moments are slightly larger for the tetragonal compounds, Ba_2CdReO_6 and Sr_2LiOsO_6, may

https://doi.org/10.1021/acs.chemmater.1c03456
Chem. Mater. 2022, 34, 1098−1109

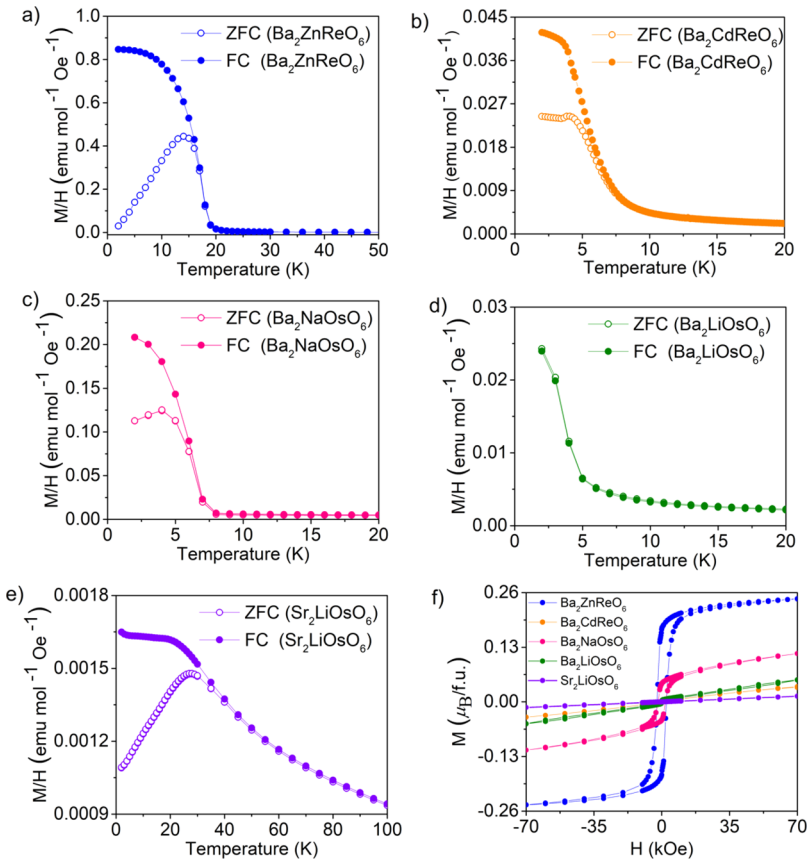

Figure 9. Temperature-dependent magnetic susceptibility for (a) Ba_2ZnReO_6, (b) Ba_2CdReO_6, (c) Ba_2NaOsO_6, (d) Ba_2LiOsO_6, and (e) Sr_2LiOsO_6 and (f) isothermal magnetization for all five compounds at 2 K.

Table 3. Ordering Temperatures as well as the Effective Moments and Weiss Constants Obtained from Curie−Weiss Fits to the High-Temperature Susceptibility Data for the $5d^1$ Double Perovskites

compound	effective moment (μ_B)	Weiss constant, θ (K)	χ_0 (emu mol^{-1} Oe^{-1})	ground state	ordering/freezing temperature
Ba_2ZnReO_6	0.7141(9)	−3.1(5)	5.1×10^{-5}	canted ferromagnet	T_C = 16 K
Ba_2LiOsO_6	0.897(1)	−55.7(6)	3.4×10^{-4}	antiferromagnet	
Ba_2CdReO_6	1.04(1)	−65.8(2)	-2.8×10^{-5}	antiferromagnet	T_N = 4 K
Ba_2NaOsO_6	0.844(1)	−41.7(6)	2.2×10^{-4}	canted ferromagnet	T_C = 7 K
Sr_2LiOsO_6	0.936(1)	−49.4(5)	2.1×10^{-4}	spin glass	T_g = 30 K

reflect partial quenching of the orbital moment due to the reduction in symmetry, but the effect is subtle.

X-ray Magnetic Circular Dichroism. To estimate the size of the spin and orbital moments, a sample of Ba_2ZnReO_6 was evaluated using XMCD. Figure 10 shows the normalized X-ray absorption (helicity-averaged) and XMCD spectra collected at the L_3 and L_2 edges of rhenium. Assuming a $5d^1$ configuration (9 holes), sum rules yield an orbital moment of $m_l = -0.40(3)$ μ_B/Re and an effective spin moment of $m_s = 1.15(5)$ μ_B/Re (the contribution of the magnetic dipole term, T_z, in the spin sum rule was neglected). The antiparallel alignment of orbital and spin moments is as expected from Hund's third rule for an ion whose available orbitals are less than half-filled. The absolute value of the spin moment exceeds the limit of 1 μ_B due to the neglect of the magnetic dipole term, but the absolute value of the orbital moment should be a reasonably reliable estimate. If we estimate the total moment to be equal to the saturated moment obtained from magnetometry (M_{sat} = 0.24 μ_B), we can make a rough estimate of 0.6−0.7 μ_B/Re for the spin moment, m_s. A similar result is obtained if we use the

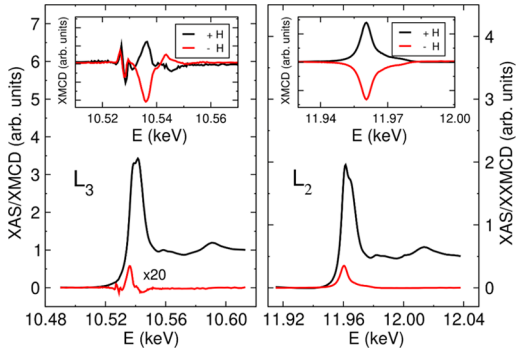

Figure 10. Main panels: normalized isotropic (helicity-averaged) and dichroic XMCD spectra at Re $L_{2,3}$ edges. Insets: dichroic XMCD spectra for opposite magnetic field directions (H = ±4 T) used to obtain "artifact-free" XMCD signals shown in the main panels. A small artifact (approx. 0.5% of absorption jump) is present in the low-energy side of the L_3-edge XMCD data.

https://doi.org/10.1021/acs.chemmater.1c03456
Chem. Mater. 2022, 34, 1098−1109

total moment of 0.2 μ_B estimated for the $5d^1$ ion Os^{7+} in Ba_2NaOsO_6 from low-temperature μSR studies.[4] Our estimates agree reasonably well with the theoretically calculated values for Ba_2NaOsO_6 of $m_l = -0.35\ \mu_B$/Re and $m_s = 0.5\ \mu_B$/Re.[32] The small moment is under the detection limit of neutron diffraction experiments described above.

Theoretical Modeling. Given the prior modeling of compounds that are nominally cubic,[14,15] here, we focus on "distorted" materials that already show an observable structural distortion at a higher temperature. Specifically, we examine the effects of two types of tetragonal distortions, either compression or elongation of the oxygen octahedron surrounding the $5d^1$ ion along the c-axis. The "spin 1/2" moments that arise from the $5d^1$ configuration interact via primarily antiferromagnetic superexchange interactions described below, but the orbitals that are occupied and the orbital degeneracy of the ground state are different for the two types of distortions. A summary of our results can also be gleaned from Figure 11.

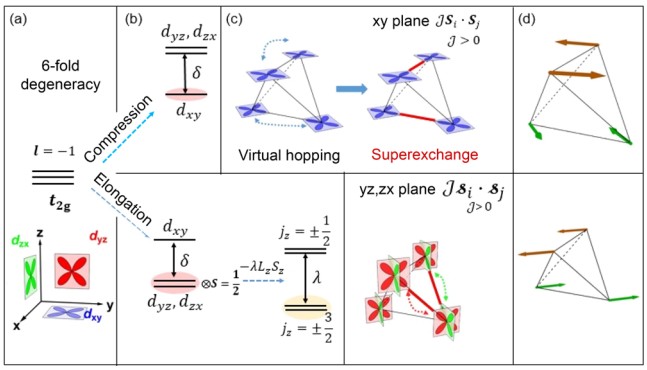

Figure 11. (a) t_{2g} orbitals, d_{xy} (blue), d_{yz} (red), and d_{zx} (green). (b) Two types of tetragonal distortions of the oxygen octahedron around the 5d ion that lifts the degeneracy in different ways for compression (top row) and elongation (bottom row) along the z-axis. (c) Virtual hopping pathways between 5d ions (dashed lines) and the resulting superexchange interactions. The dominant antiferromagnetic (AFM) interactions are shown as red bonds. (d) Resulting spin orientations in the magnetic ground state as determined from a four-site mean field theory.

Compression. We first consider the case of a uniform compression along one of the principal axes, say the z-axis, which leads to a preferential occupation of the d_{xy} orbital on every site. This is the type of distortion that occurs in Ba_2CdReO_6. Our analysis is greatly simplified compared to the cubic case[14,15] for a variety of reasons. First, the orbital angular momentum in this nondegenerate state is quenched, so we do not need to take into account the atomic spin−orbit coupling. Also, we do not need to consider the electric quadrupole−quadrupole interaction since there is no possibility of an electronically driven orbital ordering. We thus only need to derive the magnetic interaction between the $S = 1/2$ moments following the usual prescription of a strong coupling expansion in powers of the ratio of the hopping amplitude to the Hubbard U.

The largest hopping amplitude t_0 is between two orbitals in a "head-to-head configuration". This is the hopping between two d_{xy} orbitals, both of which lie in the same xy plane (blue orbital to blue orbital hopping in the xy plane in Figure 11). We neglect, to begin with, the hopping t_1 between two orbitals in a "parallel configuration", i.e., the hopping between d_{xy} orbitals in two different xy planes, since $t_1 \ll t_0$. Within this approximation, the compressed tetragonal system is described by the simple isotropic Heisenberg Hamiltonian $H_{\text{eff}} = \mathcal{J}\sum_{\langle i,j\rangle \in xy\ \text{plane}} \mathcal{S}_i \cdot \mathcal{S}_j$, where $\langle i, j\rangle$ represent nearest-neighbor (NN) $5d^1$ sites on the xy planes and the superexchange is given by $\mathcal{J} = 4t_0^2/U$. This gives rise to AFM ordering in each xy plane, but the planes are decoupled when we neglect t_1. It is easy to see that inclusion of t_1 leads to a weak AFM superexchange $\mathcal{J}' = 4t_1^2/U$ between the xy planes, which stabilizes the 3D order. Using mean field theory, we find the magnetic ground state shown in the top row Figure 11d. Note that AFM order is frustrated on the face-centered cubic lattice, and we find Neél AFM order within the xy plane and canted AFM order between xy planes with the canting angle determined by the ratio $\mathcal{J}'/\mathcal{J}$.

Elongation. Next, we consider the case of uniform elongation along the z-axis of the lattice, which lifts the three-fold degeneracy of the t_{2g} manifold to favor occupation of the doubly degenerate d_{yz}, d_{zx} orbitals. The four-fold degeneracy of this manifold is split into two doublets by the atomic spin−orbit coupling (SOC). We denote by $\mathcal{S}_i$ the "isospin 1/2" operator that acts in the lowest Kramers doublet at site i. Note that isospin $\mathcal{S}_i^z = \pm 1/2$ actually corresponds to $j_{\text{eff}} = \pm 3/2$ given the inverted sign of SOC, since the effective orbital angular momentum operator in the t_{2g} sector has a negative sign relative to the usual $\mathbf{L}$ operator.

As in the compressive case, in the elongation case too, we can ignore the electric quadrupole−quadrupole interaction that was important for the cubic materials,[14,15] since there is no possibility of an electronically driven orbital ordering. We next use a strong coupling expansion to determine the interaction between isospins $\mathcal{S}_i$ and $\mathcal{S}_j$ on NN $5d^1$ sites. As before, the hopping t_0, arising from "head-to-head configuration" of orbitals, dominates. In this case, it is hopping between d_{yz}−d_{yz} orbitals in the yz plane (red orbital to red orbital hopping in the yz plane in Figure 11) and between d_{zx}−d_{zx} orbitals in the zx plane (green orbital to green orbital hopping in the zx plane in Figure 11). We ignore the subdominant contribution arising from the hopping $t_1 \ll t_0$ between orbitals in a "parallel configuration", such as d_{yz}−d_{yz} orbitals in the xy plane (red to red orbital hopping in the xy plane), and the hopping $t_2 \ll t_0$ between orbitals in a 90° configuration, such as d_{yz}−d_{zx} orbitals in the xy plane (red to green orbital hopping within the xy plane). It is easy to see that the half-filled-to-half-filled superexchange leads to the usual AFM Heisenberg Hamiltonian for the isospins

$$H_{\text{eff}} = \mathcal{J}\sum_{\langle ij\rangle \in \{yz,zx\}} \mathcal{S}_i \cdot \mathcal{S}_j$$

in the case of elongated octahedron. As a result of the dominant hopping t_0 described above, the AFM interaction $\mathcal{J}$ acts on pairs of isospin moments connected by bonds in the xz plane (e.g., the red bond that is highlighted between the two green d_{xz} orbitals in the lower row of Figure 11c) and in the yz plane (e.g., the red bond that is highlighted between the two red d_{yz} orbitals in the lower row of Figure 11c). $\mathcal{J} \sim t_0^2/U_{\text{eff}} > 0$, where U_{eff} is the energy cost of double occupancy that can be computed by projecting the Kanamori Hamiltonian (with Hubbard U and Hunds' coupling J_H) onto the lowest Kramers'

https://doi.org/10.1021/acs.chemmater.1c03456
Chem. Mater. 2022, 34, 1098−1109

doublet. We omit the details of this calculation here since they are not relevant for the qualitative arguments presented here.

The upshot of the effective Hamiltonian described above is that we find, within mean field theory, the AFM ground state shown in the lower row in Figure 11d. This is effectively the type I AFM structure introduced in Figure 1c. We note that the AFM ground states obtained in both the distorted cases, either compression or elongation, have a zero net moment within each unit cell, distinct from a canted FM state.

To conclude, we summarize the key differences between the theoretical results presented here for the distorted $5d^1$ double perovskites with the results for cubic $5d^1$ systems.[14,15] The effective low-energy Hamiltonians in the cubic case have a complex structure involving the interplay of spin and orbital degrees of freedom, which then leads to two distinct phase transitions:[15] an electronically driven orbital ordering (or quadrupolar order) at a higher temperature T_o followed by the onset of magnetic ordering at a lower temperature T_c. In contrast, in the noncubic materials, lattice distortion leads to Kramers doublets on each transition-metal site, a simple AFM superexchange between spin or isospin-1/2 moments, and a single-phase transition to an AFM-ordered state. The AFM states for the distorted cases are in marked contrast to the prediction[14,15] of canted FM order in the cubic case.

DISCUSSION

The diversity of magnetic ground states found among double perovskites containing $5d^1$ ions is unusual. Since Re^{6+} and Os^{7+} are isoelectronic and parameters such as spin−orbit coupling and covalency are similar, it is reasonable to assume that the energies of competing magnetic ground states are highly sensitive to structural distortions. Of the nominally cubic, canted ferromagnetic double perovskites, Ba_2MgReO_6 and Ba_2NaOsO_6 have been the most extensively studied. In both compounds, there is experimental evidence for a very subtle crystallographic distortion at low temperatures. The $P4_2/mnm$ symmetry reported below 33 K for Ba_2MgReO_6 leads to three different Re−O bond lengths.[9] The Re−O bonds are elongated parallel to the *c*-axis, while in the *ab*-plane, the bonds are compressed in one direction and elongated in the other. The direction of the compressed bonds in the *ab*-plane is rotated by 90° with respect to neighboring (001) planes. This distortion, which produces a local orthorhombic symmetry, is also consistent with the peak splitting seen in low-temperature ^{23}Na NMR studies of Ba_2NaOsO_6.[8,27] Previously published theoretical modeling shows that this pattern of orbital order is essential to produce the superexchange interactions that stabilize a canted ferromagnetic state.[14,15]

The magnetism and phase transitions of Ba_2ZnReO_6 are similar to those that have been documented for Ba_2MgReO_6.[6,9] The resolution of our low-temperature NPD data is not sufficient to detect the quadrupolar orbital order that has been reported below T_q = 33 K in Ba_2MgReO_6, but there is a small feature seen at 23 K in the specific heat that may correspond to T_q. The effective moment (μ_{eff} = 0.7141(9) μ_B), negative Weiss constant (θ = −3.1(5) K), and saturated moment (M_{sat} = 0.24 μ_B/f.u.) of Ba_2ZnReO_6 are all similar to the values reported for Ba_2MgReO_6 (μ_{eff} = 0.68 μ_B, θ = −14 K, and M_{sat} = 0.3 μ_B/f.u.). We find an entropy release of 6.7 J/(mol·K) that is smaller than the value of 11.3 J/(mol·K) reported by Hirai and Hiroi on single crystals of Ba_2MgReO_6.[6] Some of the discrepancy may be due to differences in subtracting the lattice contribution to the specific heat. We use a diamagnetic analog Ba_2ZnWO_6 to estimate the lattice contribution and integrate the data up to ∼40 K, while Hirai and Hiroi fit the high-temperature data to the sum of two Debye functions and integrate the data up to 80 K.

The crystal structure and bulk magnetic properties of Ba_2NaOsO_6 are very similar to Ba_2MgReO_6 and Ba_2ZnReO_6, albeit with a slightly lower onset of magnetic order, T_C = 7 K.[2] Although no crystallographic evidence for quadrupolar orbital order has been reported, the ^{23}Na NMR spectra indicate a symmetry-lowering phase transition that is consistent with the quadrupolar phase below 13 K.[8] Here, we show that in the temperature range between T_q and T_C, the very subtle crystallographic distortion detected by NMR cannot be detected with high-resolution TOF-NPD data. This observation may help explain why it has been so difficult to find evidence for orbital order in canted ferromagnetic $5d^1$ double perovskites.

Among the nominally cubic $5d^1$ double perovskites, Ba_2LiOsO_6 is the only compound not reported to be ferromagnetic. The reasons for this anomaly remain enigmatic. The tolerance factor and lattice parameter are very similar to Ba_2MReO_6 (M = Mg and Zn). TOF-NPD data reported here indicate that Ba_2LiOsO_6 and Ba_2NaOsO_6 are isostructural at 10 K. Perhaps, Ba_2LiOsO_6 does not exhibit quadrupolar orbital order, which could be enough to stabilize a colinear antiferromagnetic state over the canted ferromagnetic state. High-resolution, low-temperature single crystal studies of the structures of Ba_2LiOsO_6 and Ba_2NaOsO_6 may help shed light on this issue. Even if it is shown that Ba_2LiOsO_6 does not have quadrupolar orbital order, why this compound behaves differently than its isoelectronic, structural doppelgangers Ba_2MReO_6 (M = Mg and Zn) would remain a mystery.

Finally, we turn our attention to the two compounds where a clear structural phase transition can be seen with conventional powder diffraction techniques: Ba_2CdReO_6 and Sr_2LiOsO_6. The theoretical modeling presented above explains the emergence of antiferromagnetism in Ba_2CdReO_6 where a cubic-to-tetragonal phase transition at 180 K leads to a compression of the Re−O bonds parallel to the *c*-axis. This distortion occurs at a much higher temperature than the cubic-to-tetragonal transition described above for Ba_2MgReO_6 and is likely driven by underbonding of the Ba^{2+} ions rather than an electronically driven distortion. This distortion results in a different space group symmetry ($I4/m$ vs $P4_2/mnm$), which leads to preferential occupation of the d_{xy} orbitals and, in turn, favors antiferromagnetic superexchange coupling within the *xy* plane as shown by theoretical modeling. The Weiss constant of −65.8 (2) K would seem to indicate that antiferromagnetic interactions within the *xy* plane are of moderate strength. The low T_N of 4 K likely arises from weak coupling between Re^{6+} ions in neighboring planes.

Curiously, the results reported in ref 7 agree with the data presented here with the exception of the magnetic ground state. In that work, the magnetic measurements provide strong support for the canted ferromagnetic state seen for the nominally cubic perovskites, unlike what is seen here. Yet both our sample and that in ref 7 are single-phase powders with nearly identical lattice parameters, and both undergo a cubic-to-tetragonal phase transition near 170 K. The only logical conclusion is that the two samples are different in some way that is not easily observed; presumably, there are subtle differences in the stoichiometry and/or defects. While both samples were prepared from similar reagents in sealed silica

https://doi.org/10.1021/acs.chemmater.1c03456
Chem. Mater. 2022, 34, 1098−1109

tubes, our sample was prepared with a slight overpressure of oxygen at 1000 °C, while the sample studied in ref 7 did not include an overpressure of oxygen and was prepared at 800 °C. This raises the possibility that the oxygen content may be nonstoichiometric, but it is very difficult to say which sample is closest to the ideal stoichiometry. However, the antiferromagnetic ordering of the sample studied here is in better agreement with the predictions of theoretical modeling.

While the tetragonal space group symmetry of Sr_2LiOsO_6 is the same as Ba_2CdReO_6, the Os-centered octahedron undergoes an axial elongation, instead of a compression. This leads to a different occupation of the 5d orbitals, a superposition of d_{zx} and d_{yz} orbitals. The other documented example of a tetragonal distortion that involves an elongation of the bonds parallel to the *c*-axis is Sr_2MgReO_6. Using a combination of NPD, muon spin resonance, specific heat, and magnetization to analyze a polycrystalline sample, Wiebe et al. concluded that Sr_2MgReO_6 was a spin glass below $T_g \approx 50$ K,[11] but a recent resonant X-ray scattering experiment on a single crystal by Gao et al. showed compelling evidence for a colinear type I AFM ($T_N = 55$ K). Here, also the competing magnetic ground states appear to be quite sensitive to subtle perturbations from defects. Theoretical modeling suggests that these compounds should adopt AFM order, like the more recent study of Sr_2MgReO_6. It should also be noted that the frustration index, 49 K/30 K ≈ 1.6, is rather small for a spin-glass ground state. It is possible in these compounds that some type of defect is responsible for local disorder that can stabilize the spin-glass state seen here for Sr_2LiOsO_6 and in the earlier studies on Sr_2MgReO_6.

CONCLUSIONS

The links between the crystal structure and the magnetism of double perovskites containing $5d^1$ transition-metal ions have been studied. Ba_2ZnReO_6 and Ba_2NaOsO_6 crystallize with the cubic double perovskite structure and retain that structure down to 10 K within the detection limits of TOF-NPD data. Both compounds adopt a canted ferromagnetic structure. Ba_2ZnReO_6 has a $T_C = 16$ K and a saturated moment of 0.24 μ_B/Re. The orbital moment is estimated to be $|m_l| = 0.4\ \mu_B$/Re by XMCD analysis. This moment opposes the spin moment, leading to a small net moment on Re of 0.2−0.3 μ_B, a value too small to be seen in the neutron powder diffraction data obtained here. Ba_2LiOsO_6 is also cubic and appears to retain the cubic structure down to 10 K but inexplicably adopts an antiferromagnetic ground state. Ba_2CdReO_6 and Sr_2LiOsO_6 are both tetragonally distorted ($I4/m$ space group symmetry) at a low temperature, but the Re−O bonds aligned parallel to the *c*-axis are compressed in the former, while analogous Os−O bonds are elongated in the latter. This distortion disrupts the quadrupolar orbital ordering that is thought to stabilize the canted ferromagnetic state, resulting in preferential occupation of the d_{xy} orbitals in Ba_2CdReO_6 and a linear combination of d_{yz} and d_{xz} orbitals in Sr_2LiOsO_6. This pattern of orbital occupation stabilizes antiferromagnetism in Ba_2CdReO_6, while Sr_2LiOsO_6 appears to be a spin glass.

ASSOCIATED CONTENT

Supporting Information

The Supporting Information is available free of charge at https://pubs.acs.org/doi/10.1021/acs.chemmater.1c03456.

SXPD refinements of Ba_2ZnReO_6 (Figure S1), SXPD refinements of Ba_2CdReO_6 (Figure S2), SXPD and NPD refinements of Sr_2LiOsO_6 (Figure S3), NPD refinements of Ba_2NaOsO_6 (Figure S4), NPD refinements of Ba_2LiOsO_6 (Figure S5), CW fit of Ba_2ZnReO_6 (Figure S6), CW fit of Ba_2CdReO_6 (Figure S7), CW fit of Sr_2LiOsO_6 (Figure S8), CW fit of Ba_2NaOsO_6 (Figure S9), CW fit of Ba_2LiOsO_6 (Figure S10), refined structural parameters of Ba_2ZnReO_6 (Table S1), refined structural parameters of Ba_2CdReO_6 (Table S2), refined structural parameters of Sr_2LiOsO_6 (Table S3), refined structural parameters of Ba_2NaOsO_6 (Table S4), and refined structural parameters of Ba_2LiOsO_6 (Table S5) (PDF)

AUTHOR INFORMATION

Corresponding Author

Patrick M. Woodward − *Department of Chemistry and Biochemistry, The Ohio State University, Columbus, Ohio 43210, United States;* orcid.org/0000-0002-3441-2148; Email: woodward.55@osu.edu

Authors

Victor da Cruz Pinha Barbosa − *Department of Chemistry and Biochemistry, The Ohio State University, Columbus, Ohio 43210, United States*

Jie Xiong − *Department of Chemistry and Biochemistry, The Ohio State University, Columbus, Ohio 43210, United States*

Phuong Minh Tran − *Department of Chemistry and Biochemistry, The Ohio State University, Columbus, Ohio 43210, United States*

Michael A. McGuire − *Materials Science and Technology Division, Oak Ridge National Laboratory, Oak Ridge, Tennessee 37831, United States;* orcid.org/0000-0003-1762-9406

Jiaqiang Yan − *Materials Science and Technology Division, Oak Ridge National Laboratory, Oak Ridge, Tennessee 37831, United States;* orcid.org/0000-0001-6625-4706

Matthew T. Warren − *Department of Physics, The Ohio State University, Columbus, Ohio 43210, United States*

Rolando Valdes Aguilar − *Department of Physics, The Ohio State University, Columbus, Ohio 43210, United States*

Wenjuan Zhang − *Department of Physics, The Ohio State University, Columbus, Ohio 43210, United States*

Mohit Randeria − *Department of Physics, The Ohio State University, Columbus, Ohio 43210, United States*

Nandini Trivedi − *Department of Physics, The Ohio State University, Columbus, Ohio 43210, United States*

Daniel Haskel − *Advanced Photon Source, Argonne National Laboratory, Lemont, Illinois 60439, United States*

Complete contact information is available at: https://pubs.acs.org/10.1021/acs.chemmater.1c03456

Notes

The authors declare no competing financial interest.

ACKNOWLEDGMENTS

The authors thank Adam Aczel for assistance with the neutron powder diffraction data on Ba_2ZnReO_6. A portion of this research used resources at the High Flux Isotope Reactor and the Spallation Neutron Source, both are DOE Office of Science User Facilities operated by the Oak Ridge National

Laboratory. The authors also thank Graham King of the Canadian Light Source for collecting synchrotron data on Sr_2LiOsO_6 and providing advice for analyzing this data. This work was supported by NSF Materials Research Science and Engineering Center (MRSEC) grants nos. DMR-1420451 and DMR-2011876. Work at Argonne is supported by the US Department of Energy, Office of Science, Office of Basic Energy Sciences, under contract no. DE-AC-02-06CH11357. Work at Oak Ridge National Laboratory was supported by the US Department of Energy, Office of Science, Basic Energy Sciences, Materials Sciences and Engineering Division, under contract no. DE-AC05-00OR22725.

REFERENCES

(1) Maharaj, D. D.; Sala, G.; Stone, M. B.; Kermarrec, E.; Ritter, C.; Fauth, F.; Marjerrison, C. A.; Greedan, J. E.; Paramekanti, A.; Gaulin, B. D. Octupolar ordering vs. Néel order in $5d^2$ double perovskites. *Phys. Rev. Lett.* **2020**, *124*, No. 087206.

(2) Stitzer, K. E.; Smith, M. D.; Zur Loye, H. C. Crystal growth of Ba_2MOsO_6 (M=Li, Na) from reactive hydroxide fluxes. *Solid State Sci.* **2002**, *4*, 311−316.

(3) Erickson, A. S.; Misra, S.; Miller, G. J.; Gupta, R. R.; Schlesinger, Z.; Harrison, W. A.; Kim, J. M.; Fisher, I. R. Ferromagnetism in the Mott Insulator Ba_2NaOsO_6. *Phys. Rev. Lett.* **2007**, *99*, 1−5.

(4) Steele, A. J.; Baker, P. J.; Lancaster, T.; Pratt, F. L.; Franke, I.; Ghannadzadeh, S.; Goddard, P. A.; Hayes, W.; Prabhakaran, D.; Blundell, S. J. Low-moment magnetism in the double perovskites Ba_2MOsO_6 (M = Li, Na). *Phys. Rev.B.* **2011**, *84*, 144416.

(5) Marjerrison, C. A.; Thompson, C. M.; Sala, G.; Maharaj, D. D.; Kermarrec, E.; Cai, Y.; Hallas, A. M.; Wilson, M. N.; Munsie, T. J. S.; Granroth, G. E.; Flacau, R.; Greedan, J. E.; Gaulin, B. D.; Luke, G. M. Cubic Re^{6+} ($5d^1$) Double Perovskites, Ba_2MgReO_6, Ba_2ZnReO_6, and $Ba_2Y_{2/3}ReO_6$: Magnetism, Heat Capacity, μSR, and Neutron Scattering Studies and Comparison with Theory. *Inorg. Chem.* **2016**, *55*, 10701−10713.

(6) Hirai, D.; Hiroi, Z. Successive Symmetry Breaking in a $J_{eff} = 3/2$ Quartet in the Spin−Orbit Coupled Insulator Ba_2MgReO_6. *J. Phys. Soc. Jpn.* **2019**, *88*, No. 064712.

(7) Hirai, D.; Hiroi, Z. Possible quadrupole order in tetragonal Ba_2CdReO_6 and chemical trend in the ground states of $5d^1$ double perovskites. *J. Phys. Condens. Matter* **2021**, *33*, 135603.

(8) Lu, L.; Song, M.; Liu, W.; Reyes, A. P.; Kuhns, P.; Lee, H. O.; Fisher, I. R.; Mitrović, V. F. Magnetism and local symmetry breaking in a Mott insulator with strong spin orbit interactions. *Nat. Commun.* **2017**, *8*, 14407.

(9) Hirai, D.; Sagayama, H.; Gao, S.; Ohsumi, H.; Chen, G.; Arima, T.; Hiroi, Z. Detection of multipolar orders in the spin-orbit-coupled *5d* Mott insulator Ba_2MgReO_6. *Phys. Rev. Res.* **2020**, *2*, No. 022063.

(10) Kato, H.; Okuda, T.; Okimoto, Y.; Tomioka, Y.; Oikawa, K.; Kamiyama, T.; Tokura, Y. Structural and electronic properties of the ordered double perovskites A_2MReO_6 (A = Sr, Ca; M = Mg, Sc, Cr, Mn, Fe, Co, Ni, Zn). *Phys. Rev. B* **2004**, *69*, 184412.

(11) Wiebe, C. R.; Greedan, J. E.; Kyriakou, P. P.; Luke, G. M.; Gardner, J. S.; Fukaya, A.; Gat-Malureanu, I. M.; Russo, P. L.; Savici, A. T.; Uemura, Y. J. Frustration-driven spin freezing in the S = 1/2 fcc perovskite Sr_2MgReO_6. *Phys. Rev. B* **2003**, *68*, 1−10.

(12) Greedan, J. E.; Derakhshan, S.; Ramezanipour, F.; Siewenie, J.; Proffen, T. A search for disorder in the spin glass double perovskites Sr_2CaReO_6 and Sr_2MgReO_6 using neutron diffraction and neutron pair distribution function analysis. *J. Phys. Condens. Matter* **2011**, *23*, 164213.

(13) Wiebe, C. R.; Greedan, J. E.; Luke, G. M.; Gardner, J. S. Spin glass behavior in the S = 1/2 fcc ordered perovskite Sr_2CaReO_6. *Phys. Rev. B* **2002**, *65*, 144413.

(14) Chen, G.; Pereira, R.; Balents, L. Exotic phases induced by strong spin-orbit coupling in ordered double perovskites. *Phys. Rev. B* **2010**, *82*, 174440.

(15) Svoboda, C.; Zhang, W.; Randeria, M.; Trivedi, N. Orbital order drives magnetic order in $5d^1$ and $5d^2$ double perovskite Mott insulators. *Phys. Rev. B* **2021**, *104*, No. 024437.

(16) Coelho, A. A. TOPAS and TOPAS-Academic: an optimization program integrating computer algebra and crystallographic objects written in C++. *J. Appl. Crystallogr.* **2018**, *51*, 210−218.

(17) Rodríguez-Carvajal, J. Recent advances in magnetic structure determination by neutron powder diffraction. *Phys. B* **1993**, *192*, 55−69.

(18) Bain, G. A.; Berry, J. F. Diamagnetic Corrections and Pascal's Constants. *J. Chem. Educ.* **2008**, *85*, 532.

(19) Thole, B. T.; Carra, P.; Sette, F.; van der Laan, G. X-Ray Circular Dichroism as a Probe of Orbital Magnetization. *Phys. Rev.Lett.* **1992**, *68*, 1943−1946.

(20) Carra, P.; Thole, B. T.; Altarelli, M.; Wang, X. X-Ray Circular Dichroism and Local Magnetic Fields. *Phys. Rev. Lett.* **1993**, *70*, 694−697.

(21) Mai, T. T.; Svoboda, C.; Warren, M. T.; Jang, T. H.; Brangham, J.; Jeong, Y. H.; Cheong, S. W.; Valdés Aguilar, R. Terahertz spin-orbital excitations in the paramagnetic state of multiferroic $Sr_2FeSi_2O_7$. *Phys. Rev. B* **2016**, *94*, 224416.

(22) Warren, M. T.; Pokharel, G.; Christianson, A. D.; Mandrus, D.; Valdés Aguilar, R. Terahertz dielectric analysis and spin-phonon coupling in multiferroic GeV_4S_8. *Phys. Rev. B* **2017**, *96*, No. 054432.

(23) Sleight, A. W.; Longo, J.; Ward, R. Compounds of osmium and rhenium with the ordered perovskite structure. *Inorg. Chem.* **1962**, *1*, 245−250.

(24) Goldschmidt, V. M. Die Gesetze der Krystallochemie. *Nature* **1926**, *21*, 477−485.

(25) Choy, J. H.; Kim, D. K.; Kim, J. Y. Study of the electronic structural variation of transition metal oxides by X-ray absorption spectroscopy. *Solid State Ionics* **1998**, *108*, 159−163.

(26) Glazer, A. M. The classification of tilted octahedra in perovskites. *Acta Cryst.* **1972**, *28*, 3384−3392.

(27) Liu, W.; Cong, R.; Reyes, A. P.; Fisher, I. R.; Mitrović, V. F. Nature of lattice distortions in the cubic double perovskite Ba_2NaOsO_6. *Phys. Rev. B* **2018**, *97*, 224103.

(28) Gao, S.; Hirai, D.; Sagayama, H.; Ohsumi, H.; Hiroi, Z.; Arima, T. Antiferromagnetic long-range order in $5d^1$ double-perovskite Sr_2MgReO_6. *Phys. Rev. B* **2020**, *101*, 220412.

(29) Yamamura, K.; Wakeshima, M.; Hinatsu, Y. Structural phase transition and magnetic properties of double perovskites Ba_2CaMO_6 (M = W, Re, Os). *J. Solid State Chem.* **2006**, *179*, 605−612.

(30) Xiong, J.; Yan, J.; Aczel, A. A.; Woodward, P. M. Type-I antiferromagnetic order in Ba_2LuReO_6: Exploring the role of structural distortions in double perovskites containing $5d^2$ ions. *J. Solid State Chem.* **2018**, *258*, 762−767.

(31) Groń, T.; Pacyna, A. W.; Malicka, E. Influence of temperature independent contribution of magnetic susceptibility on the Curie-Weiss law. *Solid State Phenom.* **2011**, *170*, 213−218.

(32) Gangopadhyay, S.; Pickett, W. E. Spin-orbit coupling, strong correlation, and insulator-metal transitions: The Jeff=3/2 ferromagnetic Dirac-Mott insulator Ba_2NaOsO_6. *Phys. Rev. B* **2015**, *91*, No. 045133.

https://doi.org/10.1021/acs.chemmater.1c03456
Chem. Mater. 2022, 34, 1098−1109